Mechanics of Advanced Materials and Structures, 15:199–207, 2008

ISSN: 1537-6494 print / 1537-6532 online
DOI: 10.1080/15376490801907673

Taylor & Francis
Taylor & Francis Group

Geometrically Exact Four-Node Piezoelectric Solid-Shell Element

G. M. Kulikov and S. V. Plotnikova
Department of Applied Mathematics and Mechanics, Tambov State Technical University, Tambov, Russia

This paper presents the geometrically exact assumed stress-strain four-node piezoelectric solid-shell element with six displacement degrees of freedom per node on the basis of the first-order equivalent single-layer theory. The proposed piezoelectric laminated shell formulation is based on the objective strain-displacement relationships, written in curvilinear reference surface coordinates, and generalizes the authors' purely mechanical finite element formulation. The mechanical and piezoelectric degrees of freedom are coupled via constitutive equations and the electric potential is assumed to be linear through the thickness of the piezoelectric layer. To overcome shear and membrane locking and have no spurious zero energy modes, the assumed strain and stress resultant fields are invoked. In order to circumvent thickness locking, the ad hoc modified laminate stiffness matrix, corresponding to the generalized plane stress condition, is employed. The elemental stiffness matrix has six zero eigenvalues and requires only direct substitutions. Moreover, it is evaluated by applying the 3D analytical integration that is economical and allows using extremely coarse meshes.

Keywords assumed stress-strain piezoelectric shell element, laminated shell, geometrically exact four-node solid-shell element, mechanical finite element formulation

1. INTRODUCTION

In recent years, considerable work has been carried out on three-dimensional (3D) continuum-based finite elements that can handle analyses of thin piezoelectric laminated composite shells satisfactorily [1, 2]. These elements are typically defined by two layers of nodes at the bottom and top surfaces of the shell with three displacement degrees of freedom per node and known as *isoparametric* piezoelectric solid-shell elements. In the isoparametric solid-shell element formulation, initial and deformed geometry are equally interpolated allowing one to describe rigid-body motions precisely. The development of piezoelectric solid-shell elements is not straightforward. In order to overcome element deficiencies such as shear, membrane, trapezoidal and thickness locking, assumed stress [3], strain [4], and stress-strain [5] finite element formulations have been used. Still, the isoparametric solid-shell element formulation is computationally inefficient because stresses and strains are analyzed in the global and local orthogonal Cartesian coordinate systems, although the normalized element coordinates represent already curvilinear convective coordinates.

An alternative way is to develop the *geometrically exact* piezoelectric solid-shell element based on the curvilinear reference surface coordinates that finds its point of departure in papers [6–8] related to the purely mechanical finite element formulation. The term *geometrically exact* reflects the fact that reference surface geometry is described by analytically given functions. The geometrically exact piezoelectric solid-shell element formulation developed is based on the principally new strain-displacement relationships of the first-order equivalent single-layer theory written in the curvilinear reference surface coordinates. It is remarkable that these strain-displacement relationships precisely represent all rigid-body motions and no assumptions except for standard Timoshenko-Mindlin kinematics are required to derive them [8]. For this purpose, displacement vectors of the bottom and top surfaces of the shell are introduced but resolved, in contrast with the isoparametric piezoelectric solid-shell formulation [3–5], in the reference surface frame.

It is assumed that the electric potential is linear through the thickness of the piezoelectric layer and all displacement and electric potential degrees of freedom are coupled via constitutive equations. This allows one to formulate efficient *curved* four-node solid-shell elements for the analysis of thin piezoelectric laminated shells. To avoid shear and membrane locking and have no spurious zero energy modes, the assumed strain and stress resultant fields are invoked. This approach was proposed by Wempner et al. [9] for the classic shear deformation shell theory and further was extended to the purely mechanical geometrically exact solid-shell element formulation [6–8].

It is known that a 6-parameter piezoelectric shell formulation on the basis of the complete 3D constitutive equations is deficient because thickness locking can occur [2]. To prevent

Accepted 3 January 2008.
The authors thank Prof. A. Benjeddou for his comments on numerical examples, which helped to improve a paper.
Address correspondence to Prof. G. M. Kulikov, Department of Applied Mathematics and Mechanics, Tambov State Technical University, Sovetskaya Street 106, Tambov 392000, Russia. E-mail: kulikov@apmath.tstu.ru

thickness locking at the finite element level the hybrid stress [3, 10] and enhanced assumed strain [5, 11] methods can be applied. In order to circumvent a locking phenomenon at the mechanical level and computational one as well, the 3D constitutive equations of piezoelectricity have to be modified [4, 12]. For this purpose, the ad hoc modified laminate stiffness matrix [13] corresponding to the generalized plane stress condition can be employed. Herein, the last approach is extended to piezoelectric crystals of monoclinic symmetry.

Taking into account that displacement vectors of bottom and top surfaces of the shell are represented in the reference surface frame, the proposed geometrically exact piezoelectric solid-shell formulation has computational advantages compared to the conventional isoparametric piezoelectric finite element formulations, since it reduces the costly numerical integration by deriving the stiffness matrix. Besides, the element stiffness matrix requires only direct substitutions, that is, no inversion is needed if sides of the element coincide with lines of principal curvatures of the reference surface and it is evaluated using the 3D analytical integration. This permits, additionally, using extremely coarse meshes. Therefore, the geometrically exact four-node solid-shell element developed is promising because electric signals generated by sensors are fed into microprocessors, which in turn must activate a system of piezoelectric actuators in *real time*.

2. TIMOSHENKO-MINDLIN KINEMATICS

Consider a shell built up in the general case by the arbitrary superposition across the wall thickness of N thin layers of uniform thickness h_k including the ℓth piezoelectric layer (PZT) as shown in Figure 1. The kth layer may be defined as a 3D body of volume V_k bounded by two surfaces S_{k-1} and S_k, located at the distances δ_{k-1} and δ_k measured with respect to the reference surface S, and the edge boundary surface Ω_k. It is assumed that the bounding surfaces S_{k-1} and S_k are continuous, sufficiently smooth and without any singularities. Let the reference surface S be referred to the orthogonal curvilinear coordinate system α_1 and α_2, which coincides with lines of principal curvatures of its surface, whereas the coordinate α_3 is oriented along the unit vector $\mathbf{e}_3$ normal to the reference surface; $\mathbf{e}_1$ and $\mathbf{e}_2$ are the tangent unit vectors to the lines of principal curvatures. Here and in the following developments the index k identifies the belonging of any quantity to the kth layer and runs from 1 to N, while the index of the piezoelectric layer $\ell = i_1, i_2, \ldots, i_L$, where L is a number of piezoelectric layers bonded to the face surfaces of the host structure or embedded into its body.

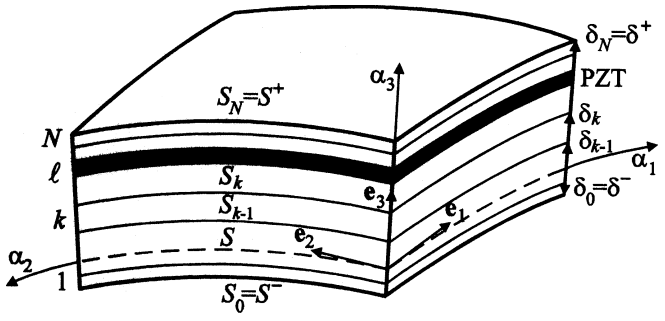

FIG. 1. Piezoelectric laminated shell.

The equivalent single-layer theory of piezoelectric shells is based on the linear approximation of displacements in the thickness direction (Timoshenko-Mindlin kinematics)

$$\mathbf{u} = N^-\mathbf{u}^- + N^+\mathbf{u}^+, \tag{1a}$$

$$\mathbf{u}^\pm = \sum_i u_i^\pm \mathbf{e}_i, \tag{1b}$$

$$N^- = \frac{1}{h}(\delta^+ - \alpha_3), \quad N^+ = \frac{1}{h}(\alpha_3 - \delta^-), \tag{1c}$$

where $\mathbf{u}^\pm(\alpha_1, \alpha_2)$ are the displacement vectors of the face surfaces; $N^\pm(\alpha_3)$ are the through-thickness shape functions of the shell; h is the thickness of the shell; the index i runs from 1 to 3.

The strain-displacement relationships can be written in the following form [8]:

$$\begin{aligned} \varepsilon_{\alpha\beta} &= N^-\varepsilon^-_{\alpha\beta} + N^+\varepsilon^+_{\alpha\beta}, \\ \varepsilon_{\alpha 3} &= N^-\varepsilon^-_{\alpha 3} + N^+\varepsilon^+_{\alpha 3}, \quad \varepsilon_{33} = \bar{\varepsilon}_{33}, \end{aligned} \tag{2}$$

where $\varepsilon^\pm_{\alpha\beta}$ and $\varepsilon^\pm_{\alpha 3}$ are the in-plane and transverse shear strains of the bottom and top surfaces of the shell defined as

$$2\varepsilon^\pm_{\alpha\beta} = \zeta^\pm_\alpha \lambda^\pm_{\alpha\beta} + \zeta^\pm_\beta \lambda^\pm_{\beta\alpha}, \quad 2\varepsilon^\pm_{\alpha 3} = \zeta^\pm_\alpha \beta_\alpha - \theta^\pm_\alpha, \quad \bar{\varepsilon}_{33} = \beta_3, \tag{3a}$$

$$\lambda^\pm_{\alpha\alpha} = \left(\frac{1}{A_\alpha} u^\pm_\alpha\right)_{,\alpha} + B_{\alpha\alpha} u^\pm_\alpha + B_{\alpha\beta} u^\pm_\beta + k_\alpha u^\pm_3 \quad (\beta \neq \alpha), \tag{3b}$$

$$\lambda^\pm_{\beta\alpha} = \left(\frac{1}{A_\alpha} u^\pm_\beta\right)_{,\alpha} + B_{\alpha\alpha} u^\pm_\beta - B_{\alpha\beta} u^\pm_\alpha \quad (\beta \neq \alpha),$$

$$\theta^\pm_\alpha = -\left(\frac{1}{A_\alpha} u^\pm_3\right)_{,\alpha} - B_{\alpha\alpha} u^\pm_3 + k_\alpha u^\pm_\alpha, \quad \beta_i = \frac{1}{h}(u_i^+ - u_i^-),$$

$$B_{\alpha\beta} = \frac{1}{A_\alpha A_\beta} A_{\alpha,\beta}, \qquad \varsigma^\pm_\alpha = 1 + k_\alpha \delta^\pm,$$

where A_α and k_α are the Lamé coefficients and principal curvatures of the reference surface; the abbreviation $()_{,\alpha}$ implies the partial derivatives with respect to coordinates α_1 and α_2; indices α, β take the values 1 and 2. It is worth noting that strain-displacement relationships (2) and (3) are very attractive because they are invariant under all rigid-body motions [8]. Note also that derivatives from Eq. (3a) have been written in a form that is best suited for applying high performance analytical integration schemes inside the element.

3. DESCRIPTION OF ELECTRIC FIELD

The electric potential inside the ℓth piezoelectric layer is also assumed to be linear in the thickness direction

$$\varphi_\ell = N_\ell^- \varphi_\ell^- + N_\ell^+ \varphi_\ell^+, \tag{4a}$$

$$N_\ell^- = \frac{1}{h_\ell}(\delta_\ell - \alpha_3), \quad N_\ell^+ = \frac{1}{h_\ell}(\alpha_3 - \delta_{\ell-1}), \tag{4b}$$

where $\varphi_\ell^\pm(\alpha_1, \alpha_2)$ are the values of the electric potential on the bottom and top surfaces of the ℓth layer; $N_\ell^\pm(\alpha_3)$ are the through-thickness shape functions of the ℓth layer.

The relation between the electric field $\mathbf{E}^{(\ell)}$ and the electric potential φ_ℓ is given as

$$\mathbf{E}^{(\ell)} = -\nabla\varphi_\ell, \tag{5a}$$

that is,

$$E_\alpha^{(\ell)} = -N_\ell^- \varphi_{\ell,\alpha}^- - N_\ell^+ \varphi_{\ell,\alpha}^+, \quad E_3^{(\ell)} = -\frac{1}{h_\ell}(\varphi_\ell^+ - \varphi_\ell^-). \tag{5b}$$

It is seen that the normal component of the electric field is constant through the thickness.

4. CONSTITUTIVE EQUATIONS

The constitutive equations of linear piezoelectricity [14, 15] for the layer treated as a crystal of monoclinic symmetry (class 2) with the second-order axis parallel to the α_3-direction can be expressed as

$$\boldsymbol{\varepsilon} = \mathbf{A}\boldsymbol{\sigma} + \mathbf{d}^{\mathrm{T}}\mathbf{E}, \tag{6}$$

$$\mathbf{D} = \mathbf{d}\boldsymbol{\sigma} + \boldsymbol{\varsigma}\mathbf{E}, \tag{7}$$

$$\boldsymbol{\sigma} = [\sigma_{11}\ \sigma_{22}\ \sigma_{33}\ \sigma_{23}\ \sigma_{13}\ \sigma_{12}]^{\mathrm{T}},$$
$$\boldsymbol{\varepsilon} = [\varepsilon_{11}\ \varepsilon_{22}\ \varepsilon_{33}\ 2\varepsilon_{23}\ 2\varepsilon_{13}\ 2\varepsilon_{12}]^{\mathrm{T}}, \tag{8}$$
$$\mathbf{D} = [D_1\ D_2\ D_3]^{\mathrm{T}}, \quad \mathbf{E} = [E_1\ E_2\ E_3]^{\mathrm{T}},$$

where $\mathbf{D}$ is the electric displacement vector; $\mathbf{A}$ is the elastic compliance matrix; $\mathbf{d}$ is the piezoelectric matrix; $\boldsymbol{\varsigma}$ is the dielectric matrix defined by

$$\mathbf{A} = \begin{bmatrix} A_{11} & A_{12} & \underline{A}_{13} & 0 & 0 & A_{16} \\ & A_{22} & \underline{A}_{23} & 0 & 0 & A_{26} \\ & & A_{33} & 0 & 0 & \underline{A}_{36} \\ & & & A_{44} & A_{45} & 0 \\ & & & & A_{55} & 0 \\ \text{sym.} & & & & & A_{66} \end{bmatrix}, \tag{9}$$

$$\mathbf{d} = \begin{bmatrix} 0 & 0 & 0 & d_{14} & d_{15} & 0 \\ 0 & 0 & 0 & d_{24} & d_{25} & 0 \\ d_{31} & d_{32} & d_{33} & 0 & 0 & d_{36} \end{bmatrix}, \quad \boldsymbol{\varsigma} = \begin{bmatrix} \varsigma_{11} & \varsigma_{12} & 0 \\ & \varsigma_{22} & 0 \\ \text{sym.} & & \varsigma_{33} \end{bmatrix}.$$

It is known that a 6-parameter piezoelectric shell formulation, based on the complete 3D constitutive equations, is deficient because thickness locking can occur [2]. This phenomenon occurs in bending dominated shell problems in the case of non-zero Poisson's ratios. Indeed, when a shell has undergone pure bending, one half of the shell body in the thickness direction is under tension and the other half is under compression. This implies that the thickness strain according to the 3D constitutive equations would be zero due to limitation of Timoshenko-Mindlin kinematics (1) and (2). Therefore, a shell will be in the plane-strain state instead of the expected plane-stress state. To circumvent these difficulties, the underlined components of the compliance matrix (9) should be set to zero [12, 13].

Following this scheme and solving constitutive Eqs. (6) for the stresses, one finds

$$\boldsymbol{\sigma} = \mathbf{C}\boldsymbol{\varepsilon} - \mathbf{e}^{\mathrm{T}}\mathbf{E}, \tag{10a}$$

$$\mathbf{C} = \tilde{\mathbf{A}}^{-1}, \quad \mathbf{e} = \mathbf{d}\mathbf{C}, \tag{10b}$$

where $\tilde{\mathbf{A}}$ is the modified compliance matrix, which answers the adopted locking-free assumption. Substituting further stresses (10a) in constitutive Eqs. (7), we derive

$$\mathbf{D} = \mathbf{e}\boldsymbol{\varepsilon} + \in\mathbf{E}, \quad \in = \varsigma - \mathbf{d}\mathbf{C}\mathbf{d}^{\mathrm{T}}. \tag{11}$$

5. HU-WASHIZU VARIATIONAL EQUATION

5.1. 3D Piezoelectric Shell Formulation

It is well known that the Hu-Washizu variational principle provides the basis for derivation of various variational principles, and many different mixed and hybrid finite elements for piezoelectric laminated shells may be designed. Herein, we consider first the most general functional depending on all field variables $\mathbf{u}$, $\boldsymbol{\varepsilon}^{\mathrm{AS}}$, $\boldsymbol{\sigma}$, $\mathbf{E}$, $\mathbf{D}$ and φ that can be expressed as follows [15, 16]:

$$\Pi_{\mathrm{HW}} = \iiint_V \Big[\frac{1}{2}(\boldsymbol{\varepsilon}^{\mathrm{AS}})^{\mathrm{T}}\mathbf{C}\boldsymbol{\varepsilon}^{\mathrm{AS}} - (\boldsymbol{\varepsilon}^{\mathrm{AS}})^{\mathrm{T}}\mathbf{e}^{\mathrm{T}}\mathbf{E} - \frac{1}{2}\mathbf{E}^{\mathrm{T}}\in\mathbf{E} - \boldsymbol{\sigma}^{\mathrm{T}}\left(\boldsymbol{\varepsilon}^{\mathrm{AS}} - \boldsymbol{\varepsilon}\right) + \mathbf{D}^{\mathrm{T}}(\mathbf{E} + \nabla\varphi) - \mathbf{b}^{\mathrm{T}}\mathbf{u}\Big]\mathrm{d}V - W,$$

$$\mathbf{u} = [u_1\ u_2\ u_3]^{\mathrm{T}}, \quad \nabla\varphi = [\varphi_{,1}\ \varphi_{,2}\ \varphi_{,3}]^{\mathrm{T}},$$
$$\mathbf{b} = [b_1\ b_2\ b_3]^{\mathrm{T}}, \ \boldsymbol{\varepsilon}^{\mathrm{AS}} = \left[\varepsilon_{11}^{\mathrm{AS}}\ \varepsilon_{22}^{\mathrm{AS}}\ \varepsilon_{33}^{\mathrm{AS}}\ 2\varepsilon_{23}^{\mathrm{AS}}\ 2\varepsilon_{13}^{\mathrm{AS}}\ 2\varepsilon_{12}^{\mathrm{AS}}\right]^{\mathrm{T}}, \tag{12}$$

where $\boldsymbol{\varepsilon}^{\mathrm{AS}}$ is the independently assumed strain vector; $\boldsymbol{\varepsilon}$ is the strain vector derived from the displacement field; $\mathbf{b}$ is the body force vector; W is the work done by external mechanical and electrical loading.

For the finite element implementation it is more convenient to reduce according to Eq. (5a) a number of field variables in the

mixed functional (12), that is,

$$\Pi_{\mathrm{HW}} = \int\!\!\int\!\!\int_V \left[\frac{1}{2}\left(\boldsymbol{\varepsilon}^{\mathrm{AS}}\right)^{\mathrm{T}}\mathbf{C}\boldsymbol{\varepsilon}^{\mathrm{AS}} + \left(\boldsymbol{\varepsilon}^{\mathrm{AS}}\right)^{\mathrm{T}}\mathbf{e}^{\mathrm{T}}\boldsymbol{\nabla}\varphi - \frac{1}{2}\left(\boldsymbol{\nabla}\varphi\right)^{\mathrm{T}}\boldsymbol{\in}\boldsymbol{\nabla}\varphi - \boldsymbol{\sigma}^{\mathrm{T}}\left(\boldsymbol{\varepsilon}^{\mathrm{AS}} - \boldsymbol{\varepsilon}\right) - \mathbf{b}^{\mathrm{T}}\mathbf{u}\right] \mathrm{d}V - W. \tag{13}$$

By invoking the stationarity of the 3D functional (13) with respect to the independent variables $\mathbf{u}$, $\boldsymbol{\varepsilon}^{\mathrm{AS}}$, $\boldsymbol{\sigma}$ and φ, the mixed variational equation for the piezoelectric shell analysis is obtained

$$\delta\Pi_{\mathrm{HW}} = 0. \tag{14}$$

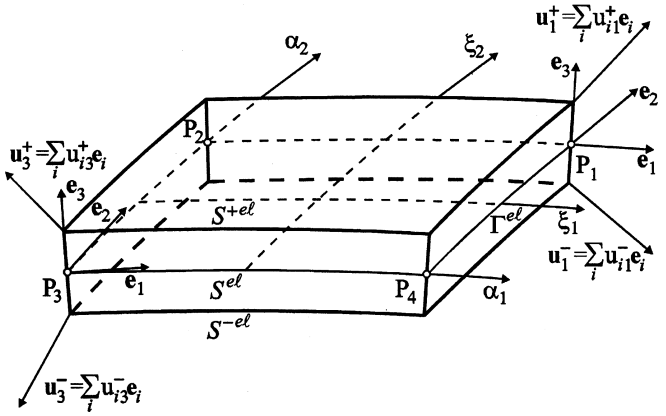

FIG. 2. Geometrically exact four-node piezoelectric solid-shell element.

5.2. 2D Piezoelectric Shell Formulation

The first-order piezoelectric laminated shell theory developed is based on the assumed approximations of displacements (1), displacement-dependent strains (2) and electric potential (4) in the thickness direction. Additionally, we have to adopt a similar approximation for the independently assumed strains

$$\begin{aligned} \varepsilon_{\alpha\beta}^{\mathrm{AS}} &= N^-\hat{\varepsilon}_{\alpha\beta}^- + N^+\hat{\varepsilon}_{\alpha\beta}^+, \\ \varepsilon_{\alpha3}^{\mathrm{AS}} &= N^-\hat{\varepsilon}_{\alpha3}^- + N^+\hat{\varepsilon}_{\alpha3}^+, \quad \varepsilon_{33}^{\mathrm{AS}} = \hat{\varepsilon}_{33}. \end{aligned} \tag{15}$$

Substituting approximations (1), (2), (4) and (15) into the Hu-Washizu mixed functional (13) and taking into account that metrics of all surfaces parallel to the reference surface are identical and equal to the metric of the midsurface, one can derive

$$\Pi_{\mathrm{HW}}^{e\ell} = \int_{-1}^{1}\int_{-1}^{1}\left[\frac{1}{2}\hat{\mathbf{E}}^{\mathrm{T}}\mathbf{D}_{\mathrm{M}}\hat{\mathbf{E}} + \hat{\mathbf{E}}^{\mathrm{T}}\mathbf{D}_{\mathrm{ME}}^{(\ell)}\boldsymbol{\Psi}_\ell + \frac{1}{2}\boldsymbol{\Psi}_\ell^{\mathrm{T}}\mathbf{D}_{\mathrm{E}}^{(\ell)}\boldsymbol{\Psi}_\ell - \mathbf{H}^{\mathrm{T}}\left(\hat{\mathbf{E}} - \mathbf{E}\right) - \mathbf{v}^{\mathrm{T}}\left(\mathbf{P}_{\mathrm{B}} + \mathbf{P}_{\mathrm{S}}\right) - \mathbf{Q}_{\mathrm{S}}^{(\ell)}\boldsymbol{\varphi}_\ell\right]\bar{A}_1^{e\ell}\bar{A}_2^{e\ell}\mathrm{d}\xi_1\mathrm{d}\xi_2. \tag{16}$$

Here, more convenient matrix notations are introduced

$$\begin{aligned} \mathbf{v} &= \left[u_1^-\ u_1^+\ u_2^-\ u_2^+\ u_3^-\ u_3^+\right]^{\mathrm{T}}, \quad \boldsymbol{\varphi}_\ell = \left[\varphi_\ell^-\ \varphi_\ell^+\right]^{\mathrm{T}}, \\ \boldsymbol{\Psi}_\ell &= \left[\boldsymbol{\varphi}_\ell^{\mathrm{T}}\ \boldsymbol{\varphi}_{\ell,1}^{\mathrm{T}}\ \boldsymbol{\varphi}_{\ell,2}^{\mathrm{T}}\right]^{\mathrm{T}}, \\ \mathbf{E} &= \left[\varepsilon_{11}^-\ \varepsilon_{11}^+\ \varepsilon_{22}^-\ \varepsilon_{22}^+\ 2\varepsilon_{12}^-\ 2\varepsilon_{12}^+\ 2\varepsilon_{13}^-\ 2\varepsilon_{13}^+\ 2\varepsilon_{23}^-\ 2\varepsilon_{23}^+\ \bar{\varepsilon}_{33}\right]^{\mathrm{T}}, \\ \hat{\mathbf{E}} &= \left[\hat{\varepsilon}_{11}^-\ \hat{\varepsilon}_{11}^+\ \hat{\varepsilon}_{22}^-\ \hat{\varepsilon}_{22}^+\ 2\hat{\varepsilon}_{12}^-\ 2\hat{\varepsilon}_{12}^+\ 2\hat{\varepsilon}_{13}^-\ 2\hat{\varepsilon}_{13}^+\ 2\hat{\varepsilon}_{23}^-\ 2\hat{\varepsilon}_{23}^+\ \hat{\varepsilon}_{33}\right]^{\mathrm{T}}, \\ \mathbf{H} &= \left[H_{11}^-\ H_{11}^+\ H_{22}^-\ H_{22}^+\ H_{12}^-\ H_{12}^+\ H_{13}^-\ H_{13}^+\ H_{23}^-\ H_{23}^+\ H_{33}\right]^{\mathrm{T}}, \\ \mathbf{Q}_{\mathrm{S}}^{(\ell)} &= \left[Q_{\mathrm{S}}^{(\ell)-}\ Q_{\mathrm{S}}^{(\ell)+}\right]^{\mathrm{T}}, \\ \hat{\mathbf{E}}\mathbf{P}_B &= \left[P_1^-\ P_1^+\ P_2^-\ P_2^+\ P_3^-\ P_3^+\right]^{\mathrm{T}}, \\ \mathbf{P}_S &= \left[-p_1^-\ \ p_1^+\ \ -p_2^-\ \ p_2^+\ \ -p_3^-\ \ p_3^+\right]^{\mathrm{T}}, \end{aligned} \tag{17}$$

where $\mathbf{D}_{\mathrm{M}}$, $\mathbf{D}_{\mathrm{ME}}^{(\ell)}$ and $\mathbf{D}_{\mathrm{E}}^{(\ell)}$ are the mechanical, piezoelectric and dielectric constitutive matrices presented in Appendix; ξ_α are the curvilinear normalized element coordinates (Figure 2); $\bar{A}_\alpha^{e\ell}$ are the Lamé coefficients of the midsurface $\bar{S}^{e\ell}$; $p_i^\pm$ are the tractions applied to the face surfaces $S^{\pm e\ell}$; $Q_S^{(\ell)\pm}$ are the prescribed surface charge densities of the ℓth piezoelectric layer; $H_{\alpha\beta}^\pm$, $H_{\alpha3}^\pm$ and H_{33} are the stress resultants; $P_i^\pm$ are the body force resultants defined as

$$H_{\alpha\beta}^\pm = \sum_k \int_{\delta_{k-1}}^{\delta_k} \sigma_{\alpha\beta}^{(k)} N^\pm \mathrm{d}\alpha_3, \qquad H_{\alpha3}^\pm = \sum_k \int_{\delta_{k-1}}^{\delta_k} \sigma_{\alpha3}^{(k)} N^\pm \mathrm{d}\alpha_3,$$
$$H_{33} = \sum_k \int_{\delta_{k-1}}^{\delta_k} \sigma_{33}^{(k)} \mathrm{d}\alpha_3, \qquad P_i^\pm = \sum_k \int_{\delta_{k-1}}^{\delta_k} b_i^{(k)} N^\pm \mathrm{d}\alpha_3. \tag{18}$$

Remark 1. For simplicity, we limit our discussion to the case of one piezoelectric layer ($\ell = i_1 \in \{1,\ 2,\ \ldots,\ N\}$) because only a sign of the summation needs to be involved in Eq. (16) to generalize.

Using the stationary of the 2D functional (16) with respect to the independent variables $\mathbf{v}$, $\hat{\mathbf{E}}$, $\mathbf{H}$ and $\boldsymbol{\varphi}_\ell$, one can write the mixed variational equation as follows:

$$\delta\Pi_{\mathrm{HW}}^{e\ell} = 0. \tag{19}$$

6. FINITE ELEMENT FORMULATION

The finite element formulation is based on the simple and efficient approximation of shells via four-node *curved* piezoelectric shell elements

$$\mathbf{v} = \sum_r N_r \mathbf{v}_r, \quad \mathbf{v}_r = \left[u_{1r}^-\ u_{1r}^+\ u_{2r}^-\ u_{2r}^+\ u_{3r}^-\ u_{3r}^+\right]^{\mathrm{T}}, \tag{20}$$

$$\hat{\mathbf{E}} = \mathbf{B}_{\mathrm{M}}\mathbf{V}, \quad \mathbf{V} = \left[\mathbf{v}_1^{\mathrm{T}}\,\mathbf{v}_2^{\mathrm{T}}\,\mathbf{v}_3^{\mathrm{T}}\,\mathbf{v}_4^{\mathrm{T}}\right]^{\mathrm{T}}, \tag{21}$$

$$\boldsymbol{\Psi}_\ell = \mathbf{B}_{\mathrm{E}}\boldsymbol{\Phi}_\ell, \quad \boldsymbol{\Phi}_\ell = \left[\boldsymbol{\varphi}_{\ell1}^{\mathrm{T}}\ \boldsymbol{\varphi}_{\ell2}^{\mathrm{T}}\ \boldsymbol{\varphi}_{\ell3}^{\mathrm{T}}\ \boldsymbol{\varphi}_{\ell4}^{\mathrm{T}}\right]^{\mathrm{T}}, \quad \boldsymbol{\varphi}_{\ell r} = \left[\varphi_{\ell r}^-\ \varphi_{\ell r}^+\right]^{\mathrm{T}}, \tag{22}$$

where $N_r(\xi_1, \xi_2)$ are the bilinear shape functions of the element; $\mathbf{v}_r$ and $\boldsymbol{\varphi}_{\ell r}$ are the displacement and electric potential vectors of the element nodes; $\mathbf{B}_{\mathrm{M}}$ is the strain-displacement transformation matrix of order 11×24; $\mathbf{B}_{\mathrm{E}}$ is the piezoelectric transformation matrix of order 6×8; the index r runs from 1 to 4 and denotes a number of nodes.

For our finite element formulation it is convenient to rewrite interpolations (21) and (22) in the following form:

$$\mathbf{E} = \sum_{r_1, r_2} \xi_1^{r_1} \xi_2^{r_2} \mathbf{B}_{\mathrm{M}}^{r_1 r_2} \mathbf{V}, \tag{23}$$

$$\boldsymbol{\Psi}_\ell = \sum_{r_1, r_2} \xi_1^{r_1} \xi_2^{r_2} \mathbf{B}_{\mathrm{E}}^{r_1 r_2} \boldsymbol{\Phi}_\ell, \tag{24}$$

where $\mathbf{B}_{\mathrm{M}}^{r_1 r_2}$ are the *constant* strain-displacement transformation matrices [7]; $\mathbf{B}_{\mathrm{E}}^{r_1 r_2}$ are the *constant* piezoelectric transformation matrices; superscripts $r_1,\ r_2$ take the values 0 and 1.

To avoid shear and membrane locking and have no spurious zero energy modes, the assumed strain and stress resultant fields inside the element [17] are introduced

$$\begin{aligned}
\hat{\boldsymbol{\varepsilon}} &= \sum_{r_1, r_2} \xi_1^{r_1} \xi_2^{r_2} \mathbf{Q}^{r_1 r_2} \hat{\mathbf{E}}^{r_1 r_2}, \\
\hat{\mathbf{E}}^{00} &= \Big[\hat{\varepsilon}_{11}^{-00}\ \hat{\varepsilon}_{11}^{+00}\ \hat{\varepsilon}_{22}^{-00}\ \hat{\varepsilon}_{22}^{+00}\ 2\hat{\varepsilon}_{12}^{-00}\ 2\hat{\varepsilon}_{12}^{+00}\ 2\hat{\varepsilon}_{13}^{-00}\ 2\hat{\varepsilon}_{13}^{+00} \\
&\qquad 2\hat{\varepsilon}_{23}^{-00}\ 2\hat{\varepsilon}_{23}^{+00}\ \hat{\varepsilon}_{33}^{00}\Big]^{\mathrm{T}}, \\
\hat{\mathbf{E}}^{01} &= \big[\hat{\varepsilon}_{11}^{-01}\ \hat{\varepsilon}_{11}^{+01}\ 2\hat{\varepsilon}_{13}^{-01}\ 2\hat{\varepsilon}_{13}^{+01}\ \hat{\varepsilon}_{33}^{01}\big]^{\mathrm{T}}, \\
\hat{\mathbf{E}}^{10} &= \big[\hat{\varepsilon}_{22}^{-10}\ \hat{\varepsilon}_{22}^{+10}\ 2\hat{\varepsilon}_{23}^{-10}\ 2\hat{\varepsilon}_{23}^{+10}\ \hat{\varepsilon}_{33}^{10}\big]^{\mathrm{T}}, \quad \hat{\mathbf{E}}^{11} = \big[\hat{\varepsilon}_{33}^{11}\big]
\end{aligned} \tag{25}$$

$$\begin{aligned}
\mathbf{H} &= \sum_{r_1, r_2} \xi_1^{r_1} \xi_2^{r_2} \mathbf{Q}^{r_1 r_2} \mathbf{H}^{r_1 r_2}, \\
\mathbf{H}^{00} &= \Big[H_{11}^{-00}\ H_{11}^{+00}\ H_{22}^{-00}\ H_{22}^{+00}\ H_{12}^{-00}\ H_{12}^{+00}\ H_{13}^{-00} \\
&\qquad \mathbf{H}_{13}^{+00}\ H_{23}^{-00}\ H_{23}^{+00}\ H_{33}^{00}\Big]^{\mathrm{T}}, \\
\mathbf{H}^{01} &= \big[H_{11}^{-01} H_{11}^{+01} H_{13}^{-01} H_{13}^{+01} H_{33}^{01}\big]^{\mathrm{T}}, \\
\mathbf{H}^{10} &= \big[H_{22}^{-10} H_{22}^{+10} H_{23}^{-10} H_{23}^{+10} H_{33}^{10}\big]^{\mathrm{T}}, \ \mathbf{H}^{11} = \big[H_{33}^{11}\big],
\end{aligned} \tag{26}$$

where $\mathbf{Q}^{00}$ is the identity matrix of order 11×11, $\mathbf{Q}^{01}$ and $\mathbf{Q}^{10}$ are the matrices of order 11×5 and $\mathbf{Q}^{11}$ is the matrix of order 11×1 from zeros and units defined in [7, 17].

Substituting interpolations (20), (23)–(26) into the mixed Eqs. (19) and (16) and using a standard variational technique, one arrives at the element equilibrium equations

$$\hat{\mathbf{E}}^{r_1 r_2} = \left(\mathbf{Q}^{r_1 r_2}\right)^{\mathrm{T}} \mathbf{B}_{\mathrm{M}}^{r_1 r_2} \mathbf{V}, \tag{27a}$$

$$\mathbf{H}^{r_1 r_2} = \left(\mathbf{Q}^{r_1 r_2}\right)^{\mathrm{T}} \mathbf{D}_{\mathrm{M}} \mathbf{Q}^{r_1 r_2} \hat{\mathbf{E}}^{r_1 r_2} + \left(\mathbf{Q}^{r_1 r_2}\right)^{\mathrm{T}} \mathbf{D}_{\mathrm{ME}}^{(\ell)} \mathbf{B}_{\mathrm{E}}^{r_1 r_2} \boldsymbol{\Phi}_\ell, \tag{27b}$$

$$\sum_{r_1, r_2} \frac{1}{3^{r_1 + r_2}} \left(\mathbf{B}_{\mathrm{M}}^{r_1 r_2}\right)^{\mathrm{T}} \mathbf{Q}^{r_1 r_2} \mathbf{H}^{r_1 r_2} = \mathbf{F}_{\mathrm{B}} + \mathbf{F}_{\mathrm{S}}, \tag{27c}$$

$$\begin{aligned}
&\sum_{r_1, r_2} \frac{1}{3^{r_1 + r_2}} \left(\mathbf{B}_{\mathrm{E}}^{r_1 r_2}\right)^{\mathrm{T}} \left(\mathbf{D}_{\mathrm{ME}}^{(\ell)\mathrm{T}} \mathbf{Q}^{r_1 r_2} \hat{\mathbf{E}}^{r_1 r_2} + \mathbf{D}_{\mathrm{E}}^{(\ell)} \mathbf{B}_{\mathrm{E}}^{r_1 r_2} \boldsymbol{\Phi}_\ell\right) \\
&= \mathbf{F}_{\mathrm{Q}}^{(\ell)},
\end{aligned} \tag{27d}$$

where $\mathbf{F}_{\mathrm{B}}$ and $\mathbf{F}_{\mathrm{S}}$ are the element-wise body and surface force vectors; $\mathbf{F}_{\mathrm{Q}}^{(\ell)}$ is the element-wise electric force vector of the ℓth piezoelectric layer.

Eliminating further assumed strains and stress resultants from Eq. (27), we obtain governing equations of the piezoelectric finite element

$$\begin{bmatrix} \mathbf{K}_{\mathrm{M}} & \mathbf{K}_{\mathrm{ME}}^{(\ell)} \\ \mathbf{K}_{\mathrm{ME}}^{(\ell)\mathrm{T}} & \mathbf{K}_{\mathrm{E}}^{(\ell)} \end{bmatrix} \begin{bmatrix} \mathbf{V} \\ \boldsymbol{\Phi}_\ell \end{bmatrix} = \begin{bmatrix} \mathbf{F}_{\mathrm{B}} + \mathbf{F}_{\mathrm{S}} \\ \mathbf{F}_{\mathrm{Q}}^{(\ell)} \end{bmatrix}, \tag{28}$$

where $\mathbf{K}_{\mathrm{M}}$ is the stiffness matrix; $\mathbf{K}_{\mathrm{ME}}^{(\ell)}$ is the piezoelectric stiffness matrix; $\mathbf{K}_{\mathrm{E}}^{(\ell)}$ is the dielectric stiffness matrix defined as

$$\begin{aligned}
\mathbf{K}_{\mathrm{M}} &= \sum_{r_1, r_2} \frac{1}{3^{r_1 + r_2}} \left(\mathbf{B}_{\mathrm{M}}^{r_1 r_2}\right)^{\mathrm{T}} \mathbf{Q}^{r_1 r_2} \left(\mathbf{Q}^{r_1 r_2}\right)^{\mathrm{T}} \\
&\qquad \mathbf{D}_{\mathrm{M}} \mathbf{Q}^{r_1 r_2} \left(\mathbf{Q}^{r_1 r_2}\right)^{\mathrm{T}} \mathbf{B}_{\mathrm{M}}^{r_1 r_2},
\end{aligned} \tag{29a}$$

$$\mathbf{K}_{\mathrm{ME}}^{(\ell)} = \sum_{r_1, r_2} \frac{1}{3^{r_1 + r_2}} \left(\mathbf{B}_{\mathrm{M}}^{r_1 r_2}\right)^{\mathrm{T}} \mathbf{Q}^{r_1 r_2} \left(\mathbf{Q}^{r_1 r_2}\right)^{\mathrm{T}} \mathbf{D}_{\mathrm{ME}}^{(\ell)} \mathbf{B}_{\mathrm{E}}^{r_1 r_2}, \tag{29b}$$

$$\mathbf{K}_{\mathrm{E}}^{(\ell)} = \sum_{r_1, r_2} \frac{1}{3^{r_1 + r_2}} \left(\mathbf{B}_{\mathrm{E}}^{r_1 r_2}\right)^{\mathrm{T}} \mathbf{D}_{\mathrm{E}}^{(\ell)} \mathbf{B}_{\mathrm{E}}^{r_1 r_2}. \tag{29c}$$

Remark 2. The element stiffness matrix $\mathbf{K}_{\mathrm{M}}$ has six zero eigenvalues as required for satisfaction of the general rigid-body motion representation, since only 18 assumed strain modes are independent of 22 ones from Eq. (25). A proof of this statement can be found in [7].

Remark 3. It is worth noting that all elemental matrices (29) require only direct substitutions, that is, no inversion is needed for the piezoelectric mixed finite element formulation developed. Furthermore, they are evaluated by using the analytical integration [7, 8]. Hence our geometrically exact piezoelectric solid-shell element formulation is very economical and efficient compared to the conventional isoparametric piezoelectric finite element formulations because it reduces the costly numerical integration by deriving elemental matrices.

For the actuator-embedded shell analysis when only a prescribed input voltage is applied, the governing finite element Eqs. (28) are simplified and expressed as

$$\mathbf{K}_{\mathrm{M}} \mathbf{V} = -\mathbf{K}_{\mathrm{ME}}^{(\ell)} \boldsymbol{\Phi}_\ell. \tag{30}$$

These equations have to be solved to assess a response of the coupled electromechanical system.

TABLE 1
Listing of piezoelectric solid-shell elements

Name	Description
GEXP4	Geometrically exact assumed stress-strain piezoelectric four-node solid-shell element developed
ISOP4	Isoparametric assumed stress piezoelectric four-node solid-shell element [3, 18]
ISOP9	Isoparametric assumed strain piezoelectric nine-node solid-shell element [4, 12]

TABLE 2
Transverse midline displacement $\bar{u}_3(10^{-7}$ m) of bimorph cantilever beam

	Dimensionless coordinate α_1/a				
	0.2	0.4	0.6	0.8	1
GEXP4 ($\nu = 0$)	0.138	0.552	1.242	2.208	3.450
Analytical [15]	0.138	0.552	1.242	2.208	3.450
ISOP4 [18]	0.138	0.552	1.242	2.208	3.450
ISOP9 [4]	0.137	0.551	1.241	2.207	3.449
GEXP4 ($\nu = 0.29$)	0.148	0.574	1.276	2.254	3.509

7. NUMERICAL EXAMPLES

The performance of the proposed geometrically exact piezoelectric solid-shell element is evaluated with several problems extracted from the literature. The results are compared with those obtained by using robust isoparametric piezoelectric solid-shell elements. A listing of these elements and the abbreviations used to identify them are contained in Table 1.

7.1. Bimorph Cantilever Beam

Consider a bimorph pointer [15] consisting of two identical PVDF layers, which have been polarized in opposite directions parallel to the thickness direction to induce internal bending moments. The geometrical and material properties of the cantilever beam are shown in Figure 3. The electrical loading case is assumed to be a unit voltage applied across the beam thickness.

The robustness of the proposed GEXP4 element is verified by solving two problems. First, we compare our results with existing beam solutions. To find such a solution, Poisson's ratio should be set to zero, i.e., we deal with problem A. Then we study the more general bimorph actuator problem B with the non-zero Poisson's ratio. Table 2 displays a distribution of the transverse displacement along the beam axis through using the 10×1 mesh of GEXP4 elements and a comparison with analytical and numerical solutions [4, 15, 18]. One can observe that our finite element formulation is completely free of thickness locking.

7.2. Simply Supported Plate with PZT Actuators

This example is presented to demonstrate the shape control of the laminated composite plate through bending actuation. A simply supported plate with PZT G1195 actuators attached to the outer surfaces is initially subjected to uniform pressure of 200 Pa [19]. The plate core is composed of six graphite/epoxy layers with stacking sequence $[0/90/0]_S$. The geometrical and material data of the problem are presented in Figure 4. The piezoceramic layers have been polarized in opposite directions and subjected to a constant voltage of $\hat{\varphi} = 15$ V and 27 V. The electrodes on the interfaces are assumed to be at the zero potential.

Due to symmetry of the problem, only one quarter of the plate is modeled by the uniform 8×8 mesh of GEXP4 elements. Figure 5 shows a distribution of the centerline transverse midplane displacement along the α_1- axis compared to results of Lee et al. [4] derived using identical node spacing. It is seen that all corresponding results are in good agreement but our code is less expensive because no matrix inversions are needed and it is based on the 3D analytical integration.

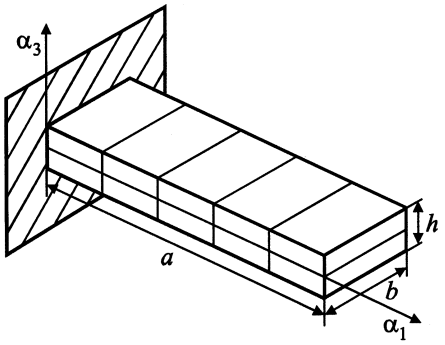

$a = 100$ mm
$b = 5$ mm
$h_1 = 0.5$ mm
$h_2 = 0.5$ mm
$h = 1$ mm
$E = 2$ GPa
$d_{31} = 23$ pm/V
$d_{32} = 23$ pm/V

Problem A: $\nu = 0$, $e_{31} = Ed_{31} = 0.046\,\mathrm{C/m^2}$, $e_{32} = e_{31}$

Problem B: $\nu = 0.29$, $e_{31} = Ed_{31}/(1-\nu) = 0.0648\,\mathrm{C/m^2}$, $e_{32} = e_{31}$

FIG. 3. Cantilever bimorph beam.

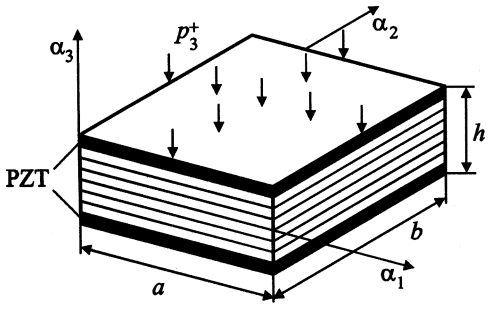

$a = 0.254$ m
$b = 0.254$ m
$h_{PZT} = 0.254$ mm
$h_C = 0.828$ mm
$h = 1.336$ mm
$p_3^+ = -200$ Pa

PZT G1195: $E = 63$ GPa, $\nu = 0.3$, $G = 24.2$ GPa,
$d_{31} = d_{32} = 254$ pm/V
Graphite/Epoxy: $E_{11} = 150$ GPa, $E_{22} = E_{33} = 9$ GPa,
$\nu_{12} = \nu_{13} = 0.3$, $G_{12} = G_{13} = 7.1$ GPa, $G_{23} = 3$ GPa

FIG. 4. Simply supported plate with PZT actuators.

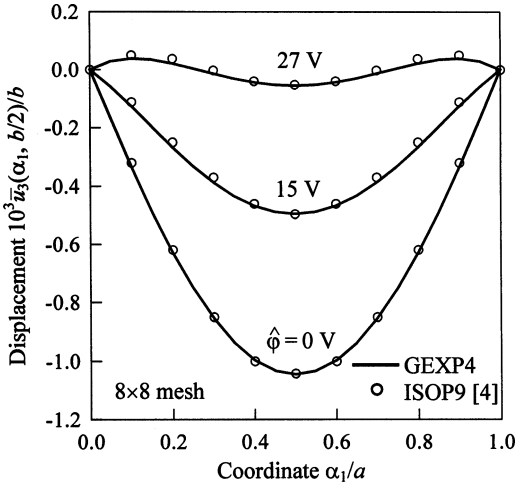

FIG. 5. Midplane displacement of simply supported plate.

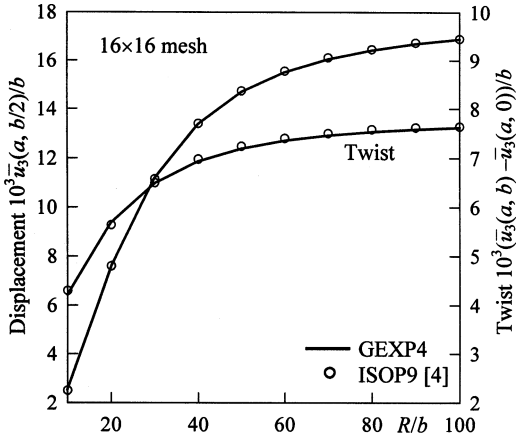

FIG. 7. Tip midsurface displacements of cantilever cylindrical shell.

7.3. Cantilever Cylindrical Shell with PZT Actuators

Further we investigate a response of the cantilever laminated cylindrical shell [19] made of the above six graphite/epoxy layers with PZT G1195 actuators bonded to the bottom and top surfaces and polarized in opposite directions parallel to the thickness direction. The material and geometrical properties of the shell are given in Figures 4 and 6, respectively. A ply orientation $[30/30/0]_S$ has been employed to induce the twisting actuation. Both piezoelectric layers are loaded statically at the outer surfaces by the same electric potential of $\hat{\varphi} = 100$ V.

Figure 7 displays the tip displacement of the midsurface and the twist, defined as a difference between two end displacement values, versus a dimensionless radius of the curvature of its surface. The results have been derived with the 16×16 mesh of geometrically exact elements developed. As can be seen, our GEXP4 element performs well again.

7.4. Cantilever Hyperbolic Shell with PVDF Actuators

To demonstrate the high coarse-mesh accuracy of the geometrically exact piezoelectric solid-shell element, we consider a six-layer graphite/epoxy hyperbolic shell covered with PVDF

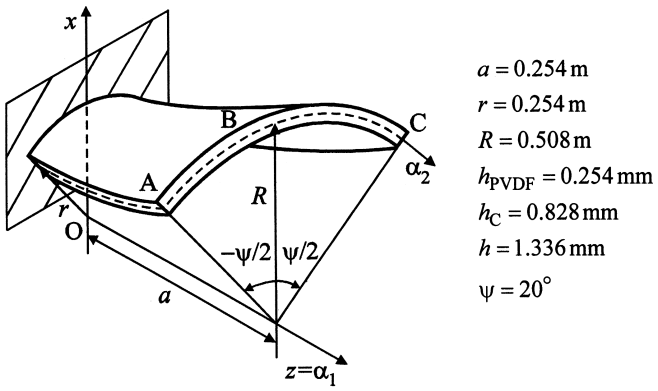

FIG. 8. Cantilever hyperbolic shell with PVDF actuators.

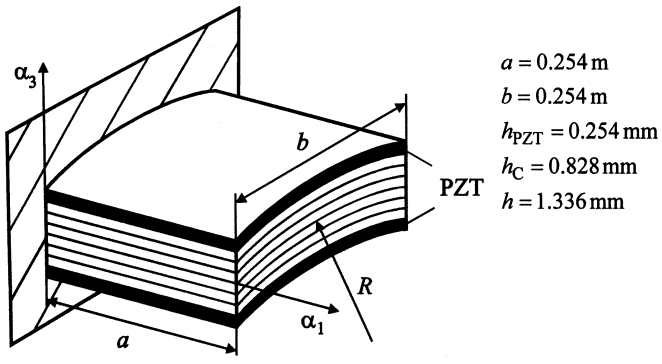

FIG. 6. Cantilever cylindrical shell with PZT actuators.

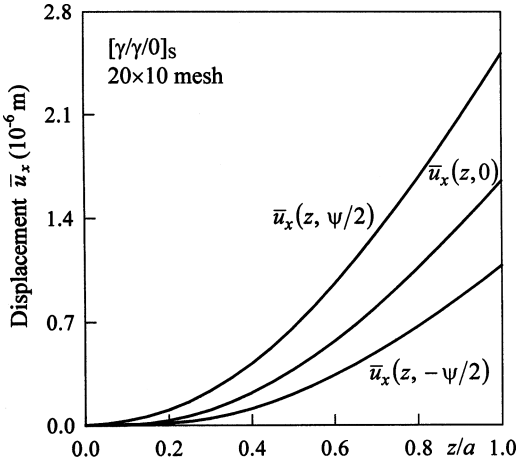

FIG. 9. Midsurface displacements of cantilever hyperbolic shell.

TABLE 3
Tip midsurface displacement $\bar{u}_x$ $\left(10^{-6}\ \mathrm{m}\right)$ of cantilever hyperbolic shell

	$[0/90/0]_S$				$[\gamma/\gamma/0]_S$			
Mesh	3×1	6×2	12×4	24×8	3×1	6×2	12×4	24×8
$\bar{u}_x^A$	0.4932	0.6001	0.6115	0.6123	1.054	0.974	1.057	1.080
$\bar{u}_x^B$		0.5421	0.5519	0.5527		1.537	1.628	1.656
$\bar{u}_x^C$	0.4932	0.6001	0.6115	0.6123	2.442	2.388	2.481	2.514

actuators on the bottom and top surfaces. A shell is assumed to be clamped on one of its edges as shown in Figure 8 and two stacking sequences $[0/90/0]_S$ and $[\gamma/\gamma/0]_S$ are studied, where γ is the angle between the asymptotic line and the tangent to the meridian. This angle is measured in the clockwise direction and may be evaluated by means of a simple formula [8]

$$\cos\gamma = \frac{A_1}{\sqrt{1+\mu}}, \qquad \mu = \frac{R^2 - r^2}{a^2}, \tag{31}$$

$$A_1 = \sqrt{1 + \frac{\mu^2 z^2}{A_2^2}}, \qquad A_2 = r\sqrt{1 + \frac{\mu z^2}{r^2}}. \tag{32}$$

The electric potential at outer surfaces of the piezoelectric layers is equal to the externally applied voltage of 1 V and at interfaces is treated as zero. Due to the opposite polarization of actuators, they will induce bending moments into the shell body and, therefore, in the case of the second ply sequence, the twisting deformation will be generated.

A shell is discretized with regular meshes of GEXP4 elements. Figure 9 shows the distribution of the midsurface displacement in the x-direction $\bar{u}_x$ along the z-axis. Additionally, Table 3 lists results of the convergence study. It should be noted that these results cannot easily be achieved by the conventional isoparametric piezoelectric solid-shell elements with such coarse mesh configuration.

8. CONCLUSIONS

A new piezoelectric laminated solid-shell model has been developed. This model is based on the objective strain-displacement relationships of the first-order equivalent single-layer theory, which are invariant under all rigid-body motions. However, the use of the proposed methodology for the finite element implementation required a modification of constitutive equations of piezoelectricity to overcome thickness locking.

The simple and efficient assumed stress-strain piezoelectric four-node *curved* solid-shell element is based on the original approach in which displacement vectors of the bottom and top surfaces are introduced but resolved, in contrast with the isoparametric solid-shell formulation, in the reference surface frame. The geometrically exact piezoelectric solid-shell element developed does not contain any spurious zero energy modes and its stiffness matrix possesses six zero eigenvalues. It is remarkable that all elemental matrices require only direct substitutions and they are evaluated by using the 3D analytical integration. So, our geometrically exact element is very economical compared to conventional isoparametric finite elements because it additionally allows using extremely coarse meshes. Taking into account that electric signals generated by sensors are fed into microprocessors to activate a system of piezoelectric actuators in real time, a developed code is robust and very promising.

REFERENCES

1. Benjeddou, A., "Advances in piezoelectric finite element modeling of adaptive structural elements: A survey," *Comput. Struct.* **76**, 347–363 (2000).
2. Sze, K. Y., "Three-Dimensional continuum finite element models for plate/shell analysis," *Prog. Struct. Eng. Mater.* **4**, 400–407 (2002).
3. Sze, K. Y., Yao, L. Q., and Yi, S., "A hybrid stress ANS solid-shell element and its generalization for smart structure modeling. Part II—Smart structure modeling," *Int. J. Numer. Meth. Eng.* **48**, 565–582 (2000).
4. Lee, S., Goo, N. S., Park, H. C., Yoon K. J., and Cho, C., "A nine-node assumed strain shell element for analysis of a coupled electro-mechanical system," *Smart Mater. Struct.* **12**, 355–362 (2003).
5. Zheng, S., Wang, X., and Chen, W., "The formulation of a refined hybrid enhanced assumed strain solid shell element and its application to model smart structures containing distributed piezoelectric sensors/actuators," *Smart Mater. Struct.* **13**, N43-N50 (2004).
6. Kulikov, G. M., and Plotnikova, S. V., "Simple and effective elements based upon Timoshenko-Mindlin Shell Theory," *Comput. Meth. Appl. Mech. Eng.* **191**, 1173–1187 (2002).
7. Kulikov G. M., and Plotnikova, S. V., "Equivalent single-layer and layerwise shell theories and rigid-body motions—Part I: Foundations, Part II: Computational aspects," *Mech. Advanced Mater. Struct.* **12**, 275–283, 331–340 (2005).
8. Kulikov, G. M., and Plotnikova, S. V., "Geometrically exact assumed stress-strain multilayered solid-shell elements based on the 3D analytical integration," *Comput. Struct.* **84**, 1275–1287 (2006).
9. Wempner, G., Talaslidis, D., and Hwang, C. M., "A simple and efficient approximation of shells via finite quadrilateral elements," *J. Appl. Mech.* **49**, 115–120 (1982).
10. Pian, T. H. H., "Finite elements based on consistently assumed stresses and displacements," *Finite Elements Anal. Des.*, **1**, 131–140 (1985).
11. Buchter, N., Ramm E., and Roehl, D., "Three-dimensional extension of nonlinear shell formulation based on the enhanced assumed strain concept," *Int. J. Numer. Meth. Eng.* **37**, 2551–2568 (1994).
12. Lee, S., Cho, B. C., Park, H. C., Yoon, K. J., and Goo, N. S., "Analysis of multilayered actuators using an assumed strain solid element," *Mater. Chem. Phys.* **75**, 174–177 (2002).
13. Ausserer, M. F., and Lee, S. W., "An eighteen-node solid element for thin shell analysis," *Int. J. Numer. Meth. Eng.* **26**, 1345–1364 (1988).

14. Cady, W. G., *Piezoelectricity: an Introduction to the Theory and Applications of Electromechanical Phenomena in Crystals*, Dover, New York (1964).
15. Tzou, H. S., *Piezoelectric Shells: Distributed Sensing and Control of Continua*, Kluwer-Academic, Dordrecht (1993).
16. Washizu, K., *Variational Methods in Elasticity and Plasticity*, 3rd ed., Pergamon Press, Oxford (1982).
17. Kulikov, G. M., and Plotnikova, S. V., "Non-linear strain-displacement equations exactly representing large rigid-body motions. Part I. Timoshenko-Mindlin shell theory," *Comput. Meth. Appl. Mech. Eng.* **192**, 851–875 (2003).
18. Sze, K. Y., and Yao, L. Q., "Modelling smart structures with segmented piezoelectric sensors and actuators," *J. Sound Vib.* **235**, 495–520 (2000).
19. Kioua, H., and Mirza, S., "Piezoelectric induced bending and twisting of laminated composite shallow shells," *Smart Mater. Struct.* **9**, 476–484 (2000).

APPENDIX

The mechanical, piezoelectric and dielectric constitutive matrices are

$$\mathbf{D}_{\mathrm{M}} = \begin{bmatrix} D_{11}^{00} & D_{11}^{01} & D_{12}^{00} & D_{12}^{01} & D_{16}^{00} & D_{16}^{01} & 0 & 0 & 0 & 0 & 0 \\ & D_{11}^{11} & D_{12}^{01} & D_{12}^{11} & D_{16}^{01} & D_{16}^{11} & 0 & 0 & 0 & 0 & 0 \\ & & D_{22}^{00} & D_{22}^{01} & D_{26}^{00} & D_{26}^{01} & 0 & 0 & 0 & 0 & 0 \\ & & & D_{22}^{11} & D_{26}^{01} & D_{26}^{11} & 0 & 0 & 0 & 0 & 0 \\ & & & & D_{66}^{00} & D_{66}^{01} & 0 & 0 & 0 & 0 & 0 \\ & & & & & D_{66}^{11} & 0 & 0 & 0 & 0 & 0 \\ & & & & & & D_{55}^{00} & D_{55}^{01} & D_{45}^{00} & D_{45}^{01} & 0 \\ & & & & & & & D_{55}^{11} & D_{45}^{01} & D_{45}^{11} & 0 \\ & & & & & & & & D_{44}^{00} & D_{44}^{01} & 0 \\ & & & & & & & & & D_{44}^{11} & 0 \\ \text{sym.} & & & & & & & & & & D_{33} \end{bmatrix},$$

$$\mathbf{D}_{\mathrm{ME}}^{(\ell)} = \begin{bmatrix} -n_\ell^0 e_{31}^{(\ell)} & n_\ell^0 e_{31}^{(\ell)} & 0 & 0 & 0 & 0 \\ -n_\ell^1 e_{31}^{(\ell)} & n_\ell^1 e_{31}^{(\ell)} & 0 & 0 & 0 & 0 \\ -n_\ell^0 e_{32}^{(\ell)} & n_\ell^0 e_{32}^{(\ell)} & 0 & 0 & 0 & 0 \\ -n_\ell^1 e_{32}^{(\ell)} & n_\ell^1 e_{32}^{(\ell)} & 0 & 0 & 0 & 0 \\ -n_\ell^0 e_{36}^{(\ell)} & n_\ell^0 e_{36}^{(\ell)} & 0 & 0 & 0 & 0 \\ -n_\ell^1 e_{36}^{(\ell)} & n_\ell^1 e_{36}^{(\ell)} & 0 & 0 & 0 & 0 \\ 0 & 0 & m_\ell^{00} e_{15}^{(\ell)} & m_\ell^{01} e_{15}^{(\ell)} & m_\ell^{00} e_{25}^{(\ell)} & m_\ell^{01} e_{25}^{(\ell)} \\ 0 & 0 & m_\ell^{10} e_{15}^{(\ell)} & m_\ell^{11} e_{15}^{(\ell)} & m_\ell^{10} e_{25}^{(\ell)} & m_\ell^{11} e_{25}^{(\ell)} \\ 0 & 0 & m_\ell^{00} e_{14}^{(\ell)} & m_\ell^{01} e_{14}^{(\ell)} & m_\ell^{00} e_{24}^{(\ell)} & m_\ell^{01} e_{24}^{(\ell)} \\ 0 & 0 & m_\ell^{10} e_{14}^{(\ell)} & m_\ell^{11} e_{14}^{(\ell)} & m_\ell^{10} e_{24}^{(\ell)} & m_\ell^{11} e_{24}^{(\ell)} \\ -e_{33}^{(\ell)} & e_{33}^{(\ell)} & 0 & 0 & 0 & 0 \end{bmatrix},$$

$$\mathbf{D}_{\mathrm{E}}^{(\ell)} = \begin{bmatrix} -h_\ell^{-1} \in_{33}^{(\ell)} & h_\ell^{-1} \in_{33}^{(\ell)} & 0 & 0 & 0 & 0 \\ & -h_\ell^{-1} \in_{33}^{(\ell)} & 0 & 0 & 0 & 0 \\ & & k_\ell^{00} \in_{11}^{(\ell)} & k_\ell^{01} \in_{11}^{(\ell)} & k_\ell^{00} \in_{12}^{(\ell)} & k_\ell^{01} \in_{12}^{(\ell)} \\ & & & k_\ell^{11} \in_{11}^{(\ell)} & k_\ell^{01} \in_{12}^{(\ell)} & k_\ell^{11} \in_{12}^{(\ell)} \\ & & & & k_\ell^{00} \in_{22}^{(\ell)} & k_\ell^{01} \in_{22}^{(\ell)} \\ \text{sym.} & & & & & k_\ell^{11} \in_{22}^{(\ell)} \end{bmatrix},$$

where

$$D_{ab}^{pq} = \sum_k n_k^{pq} C_{ab}^{(k)}, \qquad D_{mn}^{pq} = \sum_k n_k^{pq} C_{mn}^{(k)},$$

$$D_{33} = \sum_k h_k C_{33}^{(k)},$$

$$n_k^{pq} = \int_{\delta_{k-1}}^{\delta_k} (N^-)^{2-p-q} (N^+)^{p+q} d\alpha_3,$$

$$k_\ell^{pq} = -\int_{\delta_{\ell-1}}^{\delta_\ell} (N_\ell^-)^{2-p-q} (N_\ell^+)^{p+q} d\alpha_3,$$

$$m_\ell^{pq} = \int_{\delta_{\ell-1}}^{\delta_\ell} (N^-)^{1-p} (N^+)^p \left(N_\ell^-\right)^{1-q} (N_\ell^+)^q d\alpha_3,$$

where $C_{ab}^{(k)}$, $C_{mn}^{(k)}$ and $C_{33}^{(k)}$ are the stiffness coefficients of the kth layer defined in section 4; ℓ is the index of the piezoelectric layer; indices $a,\ b = 1,\ 2,\ 6$ and $m,\ n = 4,\ 5$, and $p,\ q = 0,\ 1$.